# Polarization asymmetries in the ^{9}Be(γ,n_{0}) reaction

J. M. Mueller, M. W. Ahmed, B. J. Davis, H. J. Karwowski, D. M. Markoff, L. S. Myers, M. C. Spraker, S. Stave, J. R. Tompkins, H. R. Weller, and W. R. Zimmerman

Phys. Rev. C **92**, 034604 — Published 10 September 2015

DOI: 10.1103/PhysRevC.92.034604

# Polarization Asymmetries in the $^{9}$Be($\gamma$,n$_0$) Reaction

J. M. Mueller,[1,2,3] M. W. Ahmed,[1,2,4] B. J. Davis,[4,*] H. J. Karwowski,[1,5] D. M. Markoff,[1,4] L. S. Myers,[1,2,†] M. C. Spraker,[6] S. Stave,[1,2,‡] J. R. Tompkins,[1,5,§] H. R. Weller,[1,2] and W. R. Zimmerman[1,2,7]

[1] *Triangle Universities Nuclear Laboratory, Durham, NC 27708*

[2] *Department of Physics, Duke University, Durham, NC 27708*

[3] *Department of Nuclear Engineering, North Carolina State University, Raleigh, NC 27695*

[4] *Department of Mathematics and Physics, North Carolina Central University, Durham, NC 27707*

[5] *Department of Physics and Astronomy, University of North Carolina - Chapel Hill, Chapel Hill, NC 27599*

[6] *Department of Physics, University of North Georgia, Dahlonega, GA 30597*

[7] *Department of Physics, University of Connecticut — Storrs, Storrs, CT 06269*

(Dated: August 19, 2015)

## Abstract

Measurements of the $^{9}$Be($\gamma$,$n_0$) reaction were performed using nearly 100% linearly polarized, high-intensity, and nearly-monoenergetic $\gamma$-ray beams having energies between 5.5 MeV and 15.5 MeV at the High Intensity $\gamma$-ray Source (HI$\gamma$S) located at Duke University and Triangle Universities Nuclear Laboratory. Eighteen liquid scintillator detectors were used to measure neutron yields parallel and perpendicular to the plane of beam polarization. Polarization asymmetries, which are the differences between yields observed in detectors located in-plane and out-of-plane divided by their sums, were measured for the neutrons which left the residual nucleus ($^{8}$Be) in its ground state, termed the $n_0$ group. Asymmetries between 0.4 to 0.7 were discovered over this energy region in addition to a clear trend of increasing asymmetries with increasing beam energy. A prediction of the polarization asymmetry based on a pure E1 direct capture model shows good agreement with the experimental measurements. These data and the prediction could be of interest for methods that rely on neutron measurements following photofission to identify the presence of special nuclear material.



* Present location: Department of Applied Physics, University of Michigan, Ann Arbor, MI 48109

† Present location: Thomas Jefferson National Accelerator Facility, Newport News, VA 23606

‡ Present location: Pacific Northwest National Laboratory, Richland, WA 99352

§ Present location: National Superconducting Cyclotron Laboratory, Michigan State University, East Lansing, MI 48824

## I. INTRODUCTION

$^{9}$Be has the lowest neutron separation energy (1.66 MeV) of all stable nuclides, which makes it an interesting nucleus to study in photoneutron reactions. $^{9}$Be and the deuteron are the only stable nuclides with neutron separation energies below 3 MeV, and other long-lived nuclides with separation energies below 5 MeV ($^{13}$C and $^{17}$O) have low natural abundances. The low threshold for the $^{9}$Be($\gamma$,n) reaction means that it can generate fast neutrons for $\gamma$-ray beams between 5-7 MeV, where ($\gamma$,n) reactions on other nuclei will not generate high-energy neutrons. The only other source of high-energy neutrons at these beam energies is photofission of actinide nuclei.

Recently, a new technique has been proposed to use polarization asymmetries of prompt photofission neutrons to identify the fissile or non-fissile character of samples of fissionable special nuclear material (SNM) [1, 2]. Previous experiments demonstrated that non-fissile materials that undergo polarized photofission at a beam energy of approximately 6 MeV emit a factor of 2-3 more prompt neutrons in the plane of beam polarization as compared to perpendicular to the plane of beam polarization, corresponding to polarization asymmetries between 0.4 and 0.5. As the beam energy increases, these polarization asymmetries decrease. However, at beam energies near 6 MeV, fissile materials emit approximately the same neutron yield in each plane, corresponding to polarization asymmetries near zero. Therefore, photofission with a polarized $\gamma$-ray beam has been proposed to potentially assay the fissile versus non-fissile content in a sample of SNM.

The sensitivity of this assay technique partially depends on the ability to identify potential background sources in the assay. Because $^{9}$Be has a low neutron separation energy and is a potential contaminant in a sample of SNM, the incident beam could produce fast neutrons from $^{9}$Be($\gamma$,n). If the assay is performed with neutron detectors with only coarse spectroscopic capabilities, such as organic scintillators, these fast neutrons could mimic the signal of prompt neutrons from photofission. Detailed knowledge of the fast neutrons from the $^{9}$Be($\gamma$,n) reaction is therefore required to understand the applicability of this technique. Though previous measurements of the $^{9}$Be($\gamma$,n) reaction exist, they were primarily motivated by the astrophysical implications of this reaction and did not address the energy range of interest to the assay technique nor did they use polarized $\gamma$-ray beams [3–6].

We performed measurements of the polarization asymmetries of the $n_0$ neutron group for

beam energies between 5.5 and 15.5 MeV. Here and throughout the paper the subscript $_0$ in $n_0$ refers to those neutrons which, when emitted, left the residual $^8$Be nucleus in its ground state as opposed to an excited state. We limited our analysis to these neutrons because they are the most energetic and most likely to mimic prompt fission neutrons at the lower beam energies. We also used a direct capture model of the time-reversed $^8$Be(n,$\gamma$) reaction to predict and understand the physical origin of our measured polarization asymmetries in the $^9$Be($\gamma$,$n_0$) reaction [7].

## II. EXPERIMENTAL DESCRIPTION

The High Intensity $\gamma$-ray Source (HI$\gamma$S), located at Duke University and Triangle Universities Nuclear Laboratory (TUNL), was used to generate the $\gamma$-ray beams for this experiment. The HI$\gamma$S facility is a nearly-monoenergetic Compton $\gamma$-ray source with switchable linear and circular polarizations and a wide energy range. The facility has been described in detail elsewhere [1, 8–10], so only a short description is provided here.

A nearly-monoenergetic, high-intensity $\gamma$-ray beam was created at HI$\gamma$S by colliding an electron beam in a storage ring with a high-power intra-cavity Free-Electron Laser (FEL) beam. The electron beam energy and FEL wavelength were chosen to produce $\gamma$-ray beams between 5.5 and 15.5 MeV. The energy spread (FWHM) of the beam was approximately 3% at each beam energy, and the diameter of the $\gamma$-ray beam was approximately 15 mm at the target location. The $\gamma$-ray beams were produced having either $\sim$100% circular or linear polarizations. The $\gamma$-ray beam was pulsed with a period of 179 ns, and this temporal structure enabled the use of the time-of-flight method to determine the energies of the detected neutrons.

The absolute $\gamma$-ray intensity was measured using a large NaI detector, which was periodically moved into the beam and placed behind a set of precision Cu attenuators. The measured intensity, which ranged from $3 \times 10^6$ $\gamma$/s to $2 \times 10^7$ $\gamma$/s depending on the beam energy, was continuously monitored with an array of five plastic scintillating paddles as described in Ref. [11]. The five-paddle array was calibrated using the intensity measurements from the large NaI detector.

The target was a 2.54 cm thick, 1.9 cm diameter cylindrical piece of beryllium metal, as used in Ref. [6]. This target was placed at the center of the liquid scintillator (BC-501A)

FIG. 1. (Color online) A schematic of the detector array reproduced from Ref. [1]. The detectors were located at scattering angles of $\theta = 55°, 72°, 90°, 107°, 125°$, and $142°$ and azimuthal angles of $\phi = 0°, 90°, 180°, 270°$.

detector array shown in Fig. 1. The active volume of each detector was 12.7 cm in diameter and 5.1 cm thick. Twelve detectors were placed at scattering angles $\theta = 55°$, $90°$, and $125°$, and at azimuthal angles $\phi = 0°$, $90°$, $180°$, and $270°$. The remaining six detectors were placed at $\theta = 72°$, $107°$, and $142°$, and at $\phi = 0°$ and $90°$. We defined $\phi = 0°, 180°$ as being in the plane of beam polarization and $\phi = 90°, 270°$ as being perpendicular to the plane of beam polarization. The flight path from the target to each detector was approximately 57 cm. The pulses from the detectors were processed using analog electronics built around Mesytec MPD-4 modules [12]. CAEN Analog to Digital Converters (ADCs) and Time to Digital Converters (TDCs) were used to digitize and store the outputs of the MPD-4 modules for offline analysis.

Data were first taken using a nearly 100% circularly polarized beam and then using a nearly 100% linearly polarized beam. Correction factors for instrumental asymmetries were obtained from the measurements with circularly polarized beams. The true polarization asymmetry when using a circularly polarized beam is exactly zero, so any measured asymmetries using this beam were instrumental. These instrumental effects, such as small differences in solid angle or efficiency between detectors in and out of the plane of beam polarization, or non-uniform multiple scattering within the thin target and target holder, affected the measured polarization asymmetries. Correction factors based on these instrumental asymmetries, which were typically less than ∼15%, were applied in the analysis.

## III. DATA REDUCTION AND ANALYSIS

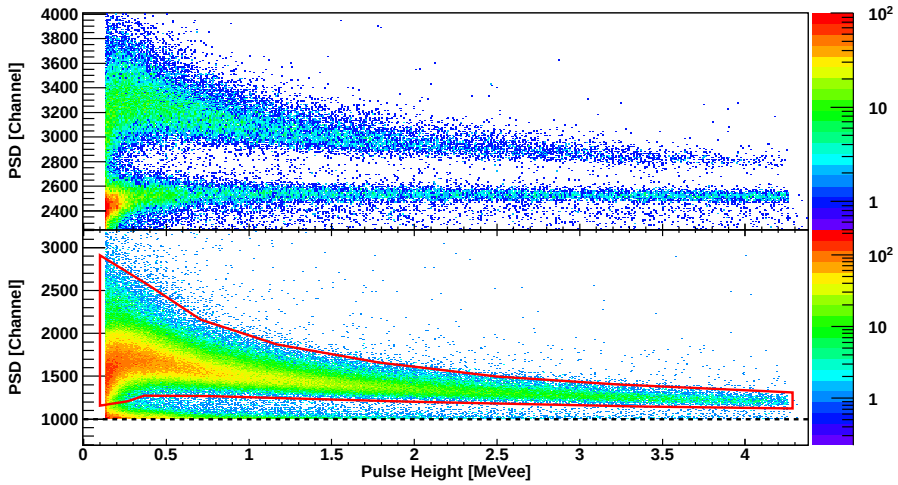


FIG. 2. (Color online) Typical two dimensional pulse height vs PSD spectra for AmBe source measurements are shown with the hardware PSD threshold in the MPD-4 module disabled (top) and enabled (bottom). The dashed line is the location of the hardware PSD threshold.

The data analysis was very similar to that described in Ref. [1], so only a brief description is given here. Detector pulse heights were calibrated using a $^{137}$Cs source, and the detector thresholds were set to $^1/_4\times$Cs. Source runs were also taken using an AmBe source to set the pulse shape discrimination (PSD) parameters used by the MPD-4 modules to discriminate $\gamma$ rays from neutrons. Cables with well-known delay times were used to calibrate the TDCs and determine the appropriate conversion from number of TDC channels into nanoseconds.

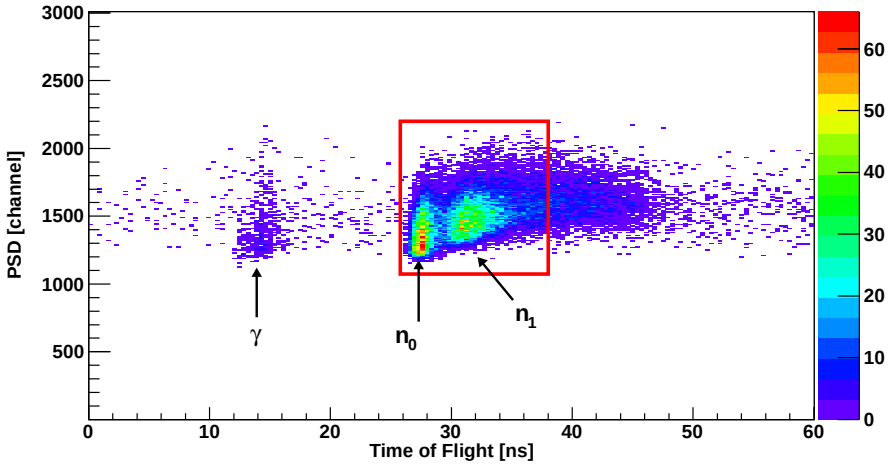


FIG. 3. (Color online) A typical two dimensional time-of-flight vs PSD spectrum is shown for a beam energy of 10 MeV and a scattering angle of 90°. Some $\gamma$-ray events are visible at early time-of-flights, and both the $n_0$ and $n_1$ groups are observed at later time-of-flights.

After the calibrations were performed, multiple cuts were applied to the data to extract the neutron yields in each detector. The first cut applied was a two dimensional cut in pulse height and PSD as shown in Fig. 2. This cut was set using an AmBe source, and the purpose of this cut was to eliminate the majority of $\gamma$-ray events in the detector. After using this cut, a single cut in both PSD and time-of-flight was applied. This cut, shown in Fig. 3, removed nearly all remaining $\gamma$-ray backgrounds.

The energies of the detected neutrons could be determined from their time of flight by measuring the distance from the target to the detector and using the time of arrival of $\gamma$ rays in the detector. The monoenergetic neutrons from the $^9$Be($\gamma$,$n_0$) reaction were used to make slight adjustments to the detector distances to correct for the finite thickness of the active volume of the detectors. The resulting neutron energy resolution was approximately 10%.

The $n_0$ yields were then extracted by summing all measured counts above a minimum energy threshold which was set to eliminate multiple-scattered neutrons and the $n_1$ group, which are neutrons that left the residual $^8$Be nucleus in its first excited state. The threshold was typically chosen by fitting the $n_0$ group to a Gaussian distribution and moving down one standard deviation in energy from the centroid. Figure 4 shows the energy spectrum and threshold at a scattering angle of $\theta = 90°$ and a beam energy of 10.0 MeV. The energy

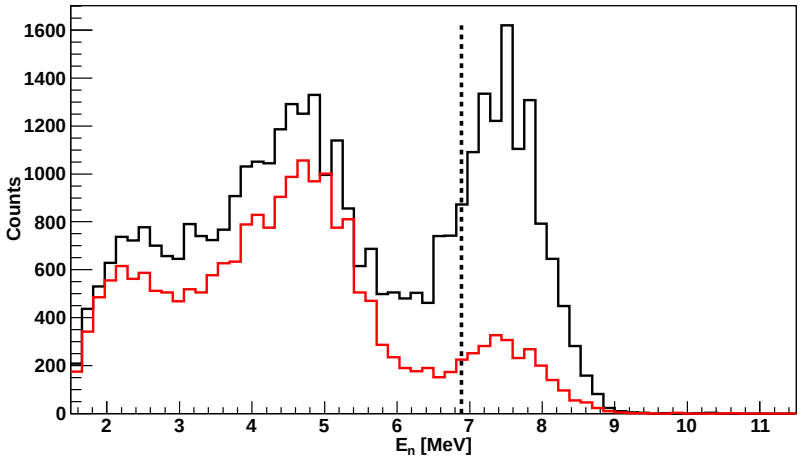


FIG. 4. (Color online) The neutron energy spectrum is shown for a linearly polarized beam at an energy of 10.0 MeV for two detectors: one in the plane of beam polarization (black, upper histogram) and the other perpendicular to the plane of beam polarization (red, lower histogram). Both detectors were located at a scattering angle of $\theta = 90°$. The dashed line indicates the placement of the energy cut to eliminate the $n_1$ group.

cut eliminates the $n_1$ group and a clear difference in $n_0$ yields between the two detectors is observed.

The polarization asymmetry was determined at each scattering angle $\theta$ by first normalizing the linearly-polarized beam yield in each detector to its circularly-polarized beam yield under the same neutron cuts. This procedure eliminated the instrumental asymmetries discussed in Section II. Then, the polarization asymmetry was taken as:

$$\Sigma(\theta) = \frac{\sum_{\phi=0°,180°} Y(\theta,\phi) - \sum_{\phi=90°,270°} Y(\theta,\phi)}{\sum_{\phi=0°,180°} Y(\theta,\phi) + \sum_{\phi=90°,270°} Y(\theta,\phi)}, \tag{1}$$

where $Y(\theta,\phi)$ is the normalized yield in the detector located at a scattering angle $\theta$ and azimuthal angle $\phi$. The resulting polarization asymmetries had both statistical and systematic uncertainties. The systematic uncertainties were largely due to the statistical uncertainty on the circularly-polarized beam yield. Then, under the assumption of pure electric dipole (E1) radiation, the polarization asymmetry as a function of $\theta$ was expressed in terms of a single coefficient ($b$) as previously given in Ref. [1] :

$$\Sigma(\theta) = \frac{b\sin^2\theta}{1 - b + b\sin^2\theta}, \tag{2}$$

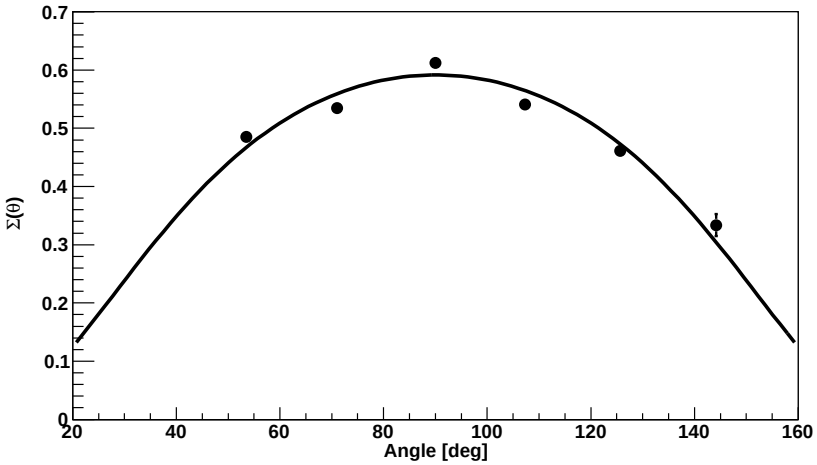


FIG. 5. The measured polarization asymmetries $\Sigma(\theta)$ at a beam energy of 10.0 MeV are fit using Eq. 2. The uncertainties are statistical and systematic combined. Uncertainties not shown are smaller than the size of the data points.

where $b$ is the angular distribution coefficient as given by

$$W(\theta, \phi) = a + b \sin^2 \theta + P_\gamma b \cos 2\phi \sin^2 \theta, \tag{3}$$

where $W(\theta, \phi)$ represents the angular distribution and $P_\gamma$ is the polarization of the $\gamma$-ray beam, which was taken as 1.0. The normalization chosen was $a + b = 1$. The $b$ coefficient is equivalent to the polarization asymmetry at a scattering angle of $\theta = 90°$. Fits were performed with a quadrupole term ($\sin^2(2\theta)$) in addition to the dipole term ($\sin^2(\theta)$), and for all beam energies the quadrupole coefficient was found to be negligible. The quadrupole coefficient ranged between -0.04 and 0.02 and the typical uncertainty on the quadrupole coefficient was approximately 0.02. Therefore, the quadrupole contribution was removed and the final fits were performed with only the electric dipole contribution. Figure 5 shows an example fit at a beam energy of 10.0 MeV.

Finally, the impact of the neutron energy cut on the extracted $b$ value was assessed by varying the location of the cut. The cut was varied between one standard deviation below the $n_0$ peak and the centroid of the $n_0$ peak. The entire analysis procedure was performed with these different cut locations, and the variation in the extracted $b$ coefficient was taken as its systematic uncertainty. The resulting systematic uncertainty was approximately the same size as the statistical uncertainty on $b$.

## IV. RESULTS

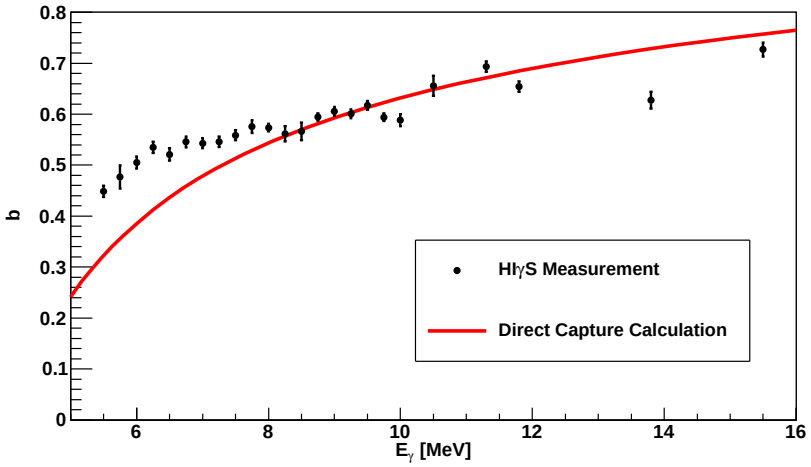


FIG. 6. (Color online) The measured $b$ values as a function of beam energy (black points) are compared to the results of the calculation (red line). The uncertainties shown are statistical and systematic combined.

Figure 6 shows the extracted $b$ coefficients as a function of beam energy. Overall, significant $b$ values (or equivalently polarization asymmetries at a scattering angle of $\theta = 90°$) are observed at all beam energies. There is a clear trend of increasing $b$ values with increasing beam energy. The $b$ values at beam energies around 6 MeV are comparable to those measured in photofission of $^{232}$Th and $^{238}$U [1], but the increase in $b$ value with increasing beam energy is a very different behavior from that observed in prompt photofission neutrons, where the $b$ values quickly tend to zero with increasing beam energy.

## V. DIRECT CAPTURE CALCULATION

A calculation based on a direct capture model was performed in an attempt to understand the origin of the magnitude and the energy dependence of the large measured polarization asymmetries in the $^{9}$Be($\gamma$,n$_0$)$^{8}$Be reaction. The direct capture model describes the direct capture of a nucleon by a target nucleus with the subsequent emission of a $\gamma$ ray, as discussed in detail in Refs. [13, 14]. In the present case we applied this model to the photodisintegration reaction $^{9}$Be($\gamma$,n$_0$)$^{8}$Be, which is the time-reverse of the capture reaction. Time reversal

TABLE I. Parameters of the direct capture model

| Bound State Parameters | Values |
|---|---|
| $V_B$ | 43.0 MeV |
| $r_B$ | 1.17 fm |
| $a_B$ | 0.75 fm |
| **Optical Model Parameters** | **Values** |
| $V_{OM}$ | 40.7 MeV |
| $W_S$ | 22.2 MeV |
| $V_{SO}$ | 6.25 MeV |
| $r_{OM}$, $r_S$, $r_{SO}$ | 1.40 fm |
| $a_{OM}$, $a_{SO}$ | 0.62 fm |
| $a_S$ | 0.39 fm |

invariance shows that the resulting transition matrix elements (TMEs) are identical for these two reactions.

The evaluation of the direct-capture TMEs begins with the assumption of pure electric dipole (E1) radiation and the use of the long-wavelength approximation. Under these assumptions, there are three complex TMEs for the case of E1 $\gamma$ rays incident on a $^9$Be target. Since the ground state of $^9$Be has a spin and parity of $^3/_2^-$, the E1 photon can excite states having $J^\pi$ values of $^1/_2^+$, $^3/_2^+$, or $^5/_2^+$. These states can subsequently transition to the $0^+$ ground state of $^8$Be by emitting neutrons having ($l$, $j^\pi$) values of (0, $^1/_2^+$), (2, $^3/_2^+$), or (2, $^5/_2^+$). We label the three complex TMEs by the incident multipolarity and the ($l$, $j^\pi$) values of the outgoing neutrons:

$$\mathrm{E1}(0, {}^1/_2^+) \rightarrow \mathcal{M}_1 e^{i\delta_1} \tag{4}$$

$$\mathrm{E1}(2, {}^3/_2^+) \rightarrow \mathcal{M}_3 e^{i\delta_3} \tag{5}$$

$$\mathrm{E1}(2, {}^5/_2^+) \rightarrow \mathcal{M}_5 e^{i\delta_5} \tag{6}$$

The evaluation of these TMEs requires calculating the radial matrix elements of the form:

$$\langle u_{l_b j_b} |\, r \,| \chi_{lj} \rangle \tag{7}$$

where $u_{l_b j_b}$ represents the radial wavefunction of the single particle (neutron) bound state in $^9$Be having quantum numbers $l_b = 1$ and $j_b = {}^3/_2$, and $\chi_{lj}$ represents the radial part

of the continuum wavefunction of the outgoing neutrons. The single particle bound state wavefunction was generated by means of a real Woods-Saxon potential whose well depth was adjusted to reproduce the binding energy of a neutron in $^9$Be ($E_B$ = 1.67 MeV). The values of the well depth ($V_B$) along with the radius and diffuseness parameters ($r_B$ and $a_B$, respectively) are presented in Table I.

The continuum wavefunctions of the outgoing neutrons (or incoming for the capture reaction) are labeled by their $lj$ values, the same labels as used for the case of the TMEs. The radial parts of these wavefunctions, $\chi_{lj}$, were generated by means of an Optical Model Potential (OMP). The parameters for this potential were primarily taken from Ref. [15], which gives an OMP obtained by fitting cross section data from the $^9$Be(n,n) reaction at 14 MeV and is a reasonable approximation to the present case. The depth, radius, and diffuseness parameters of the real potential ($V_{OM}$, $r_{OM}$, and $a_{OM}$), the surface imaginary potential ($W_S$, $r_S$, and $a_S$), and the spin-orbit potential ($V_{SO}$, $r_{SO}$, and $a_{SO}$) are presented in Table I.

The HIKARI code developed at TUNL can be used to calculate direct capture matrix elements [16]. It performs this calculation by generating bound state wavefunctions using the bound state parameters and scattering wavefunctions from the optical model parameters. Then, it evaluates the radial matrix element given in Eq. 7. Following this, the complex transition matrix elements were calculated following Eq. 26 of Ref. [14].

The formalism and tables of Ref. [7] were then used to obtain the expression for the polarization asymmetry in terms of the three E1 TMEs described above. Letting $\delta_{pq} = \delta_p - \delta_q$, we can write the equation for the polarization asymmetry at $\theta = 90^\circ$ as:

$$\Sigma_n(90^\circ) = b = 2.324\ \frac{\begin{pmatrix} 0.153\mathcal{M}_1\mathcal{M}_3\cos(\delta_{13}) + 0.563\mathcal{M}_1\mathcal{M}_5\cos(\delta_{15}) \\ - 0.356\mathcal{M}_3\mathcal{M}_5\cos(\delta_{35}) + 0.194\left(\mathcal{M}_3\right)^2 \\ - 0.290\left(\mathcal{M}_5\right)^2 \end{pmatrix}}{\begin{pmatrix} 0.119\mathcal{M}_1\mathcal{M}_3\cos(\delta_{13}) + 0.436\mathcal{M}_1\mathcal{M}_5\cos(\delta_{15}) \\ - 0.276\mathcal{M}_3\mathcal{M}_5\cos(\delta_{35}) - 0.375\left(\mathcal{M}_1\right)^2 \\ - 0.600\left(\mathcal{M}_3\right)^2 - 1.350\left(\mathcal{M}_5\right)^2 \end{pmatrix}} \tag{8}$$

The result of this calculation is shown in Fig. 6. It is worth noting that the parameters presented in Table I were not fit to the experimental results. The good agreement with the

data, especially for energies at and above 8 MeV, indicates that the observed polarization asymmetries are well described by the (inverse) direct capture model in this energy region. The disagreement for beam energies below 8 MeV suggests that the optical model potential may be inaccurate at these energies or that the simple direct-capture mechanism is not adequate here.

## VI. CONCLUSIONS

The polarization asymmetries in the neutrons from the $^{9}$Be($\gamma$,$n_0$) reaction were measured for $\gamma$-ray beam energies between 5.5 and 15.5 MeV. These asymmetries were found to be quite large, ranging between 0.4 and 0.7, and they increased with beam energy. The measured asymmetries are in fair agreement with predictions based on a direct capture model using only E1 contributions. The polarization asymmetries at 6 MeV are comparable to those from photofission of non-fissile actinides, but the asymmetries from $^{9}$Be($\gamma$,$n_0$) increase as the beam energy increases, while the asymmetries from photofission decrease with increasing beam energy [1]. This significantly different behavior from fissionable nuclei, along with the low photoneutron threshold, constitute a unique signature for the presence of $^{9}$Be. The measured asymmetries and their modeling are important to understanding potential backgrounds for a new method of assaying SNM.

## VII. ACKNOWLEDGEMENTS

The authors wish to thank the HI$\gamma$S staff for the high quality beams produced during this experiment. The authors also wish to thank J. S. Hauver, W. Henderson, J. Silano, and K. Thrasher for their help in aligning and calibrating the neutron detectors.

This work was supported in-part by DNDO, Academic Research Initiative (ARI) Grant # 2010-DN-077-ARI46-02, ARI Grant # 2008-DN-077-ARI010, DOE Grant # DE-AC52-07NA27344, DOE Grant # DE-AC02-05CH11231, NSF CREST Award HRD 0833184, and by the DOE Office of Science Graduate Fellowship Program (DOE SCGF), made possible in part by the American Recovery and Reinvestment Act of 2009, administered by ORISE-

ORAU under contract # DE-AC05-06OR23100.

---

[1] J. M. Mueller, M. W. Ahmed, R. H. France, M. S. Johnson, H. J. Karwowski, L. S. Myers, J. Randrup, M. H. Sikora, M. C. Spraker, S. Stave, J. R. Tompkins, R. Vogt, H. R. Weller, C. S. Whisnant, and W. R. Zimmerman, Physical Review C **89**, 034615 (2014).

[2] J. M. Mueller, M. W. Ahmed, and H. R. Weller, Nuclear Instruments and Methods in Physics Research Section A: Accelerators, Spectrometers, Detectors and Associated Equipment **754**, 57 (2014).

[3] B. Fabricand, B. Allison, and J. Halpern, Physical Review **103**, 1755 (1956).

[4] R. Bosch, J. Lang, R. Muller, and W. Wolfli, Helvetica Physica Acta **36**, 657 (1963).

[5] K. Sumiyoshi, H. Utsunomiya, S. Goko, and T. Kajino, Nuclear Physics A **709**, 467 (2002).

[6] C. W. Arnold, T. B. Clegg, C. Iliadis, H. J. Karwowski, G. C. Rich, J. R. Tompkins, and C. R. Howell, Physical Review C **85**, 044605 (2012).

[7] H. Weller, J. Langenbrunner, R. Chasteler, E. Tomusiak, J. Asai, R. Seyler, and D. Lehman, Atomic Data and Nuclear Data Tables **50**, 29 (1992).

[8] V. N. Litvinenko, B. Burnham, M. Emamian, N. Hower, J. Madey, P. Morcombe, P. O'Shea, S. Park, R. Sachtschale, K. Straub, G. Swift, P. Wang, Y. Wu, R. Canon, C. Howell, N. Roberson, E. Schreiber, M. Spraker, W. Tornow, H. Weller, I. Pinayev, N. Gavrilov, M. Fedotov, G. Kulipanov, G. Kurkin, S. Mikhailov, V. Popik, A. Skrinsky, N. Vinokurov, B. Norum, A. Lumpkin, and B. Yang, Physical Review Letters **78**, 4569 (1997).

[9] H. R. Weller, M. W. Ahmed, H. Gao, W. Tornow, Y. K. Wu, M. Gai, and R. Miskimen, Progress in Particle and Nuclear Physics **62**, 257 (2009).

[10] A. M. Bernstein, M. W. Ahmed, S. Stave, Y. K. Wu, and H. R. Weller, Annual Review of Nuclear and Particle Science **59**, 115 (2009).

[11] R. Pywell, O. Mavrichi, W. Wurtz, and R. Wilson, Nuclear Instruments and Methods in Physics Research Section A: Accelerators, Spectrometers, Detectors and Associated Equipment **606**, 517 (2009).

[12] A. Ruben, T. E. Hoagland, R. Fox, P. L. Kerr, G. Montermann, and R. Schneider, IEEE Nuclear Science Symposium Conference Record **1**, 681 (2007).

[13] C. Rolfs, Nuclear Physics A **217**, 29 (1973).

[14] H. R. Weller and N. R. Roberson, Reviews of Modern Physics **52**, 699 (1980).

[15] H. Lutz, J. Mason, and M. Karvelis, Nuclear Physics **47**, 521 (1963).

[16] H. Kitazawa, Private communication (1980).